J Inno Sci Eng, 2026, 10(2):248-257

DOI:https://doi.org/10.38088/jise.1755482

Research Article

# Design of a High-Efficiency, Polarization-Insensitive Quad-Band Metasurface Absorber for Microwave Applications

**Merve Kurt [1*], Gökhan Öztürk [1]**

[1] *Department of Electrical-Electronics, Atatürk University, 25240 Erzurum, Türkiye*

ARTICLE INFO

Received Date: 1/08/2025
Accepted Date: 13/01/2026

Cite this paper as:
Kurt, M., & Öztürk G. (2026). Design of a High-Efficiency, Polarization-Insensitive Quad-Band Metasurface Absorber for Microwave Applications. *Journal of Innovative Science and Engineering.* 10(2), 248-257.

*Corresponding author: Merve Kurt
E-mail:merve.kurt025@gmail.com

*Keywords:*
Electromagnetic absorption
CST Microwave Studio
Advanced Design System
Equivalent circuit model

© Copyright 2026 by
Bursa Technical University. Available online at http://jise.btu.edu.tr/

The works published in Journal of Innovative Science and Engineering (JISE) are licensed under a Creative Commons Attribution-NonCommercial 4.0 International License.

## ABSTRACT

In this study, a multi-band, high-absorption, polarization- and angle-insensitive metasurface absorber (MSA) was designed for potential use in defense industry applications. In this context, a metasurface absorber capable of achieving high absorption at four distinct resonance frequencies was proposed. Electromagnetic (EM) simulations of the proposed metasurface absorber (MSA) were performed using CST Microwave Studio (CST). According to the simulation results, the absorber achieved absorption rates of 99.8%, 99.9%, 96.9%, and 99.02% at 3.5 GHz, 7.1 GHz, 9.4 GHz, and 13.7 GHz, respectively. These resonance frequencies correspond to the S, C, X, and Ku bands, demonstrating that the design effectively operates across four different microwave bands and exhibits strong multi-band absorption characteristics. Due to the symmetric geometry of the metamaterial structure, the absorber exhibited nearly identical performance under both TE and TM polarization modes, confirming the polarization-insensitive behavior of the proposed design. Furthermore, angular stability analysis revealed that the absorber maintained absorption levels above 80% for incident angles up to 60°, indicating strong robustness and angle insensitivity. To provide a deeper understanding of the absorption mechanism, detailed analyses were conducted on the structure's characteristic impedance, surface current distributions, and electric and magnetic field intensities at each resonance frequency. Additionally, to validate the simulation accuracy, an equivalent circuit model (ECM) of the proposed metasurface absorber was developed using the Advanced Design System (ADS), and the results were compared with those obtained from CST simulations.

## 1. Introduction

Metamaterial absorbers (MMA) have recently become a significant research topic in various fields such as electromagnetic (EM) and microwave applications. The first important study in this area was conducted by Landy et al., who designed the first metamaterial absorber achieving high absorption (Landy et al., 2008). The concept of metamaterials was initially proposed theoretically by Veselago in the 1960s. Veselago suggested that materials exhibiting simultaneously negative electric permittivity (ε) and negative magnetic permeability (μ) could possess a negative refractive index. These theoretical predictions were later experimentally validated by Pendry et al. In 1998, they demonstrated structures with negative electric permittivity (Pendry et al., 1998), followed by structures exhibiting negative magnetic permeability in 1999 (Pendry et al., 1999). By combining these two properties,

metamaterials were realized, enabling their fabrication and use in EM applications.

Metamaterials, owing to their unique EM properties that do not exist in nature, enable effective control over the propagation, direction, frequency, and polarization characteristics of EM waves (Y. Wang et al., 2019). With these distinct features, metamaterials have gained significant prominence in various application fields such as the defense industry (Singh & Gupta, 2022), telecommunications (Meenakshi et al., 2022), biomedical engineering (Chen et al., 2025), and image processing (Padilla & Averitt, 2022). Moreover, they are widely utilized in the design of functional structures such as wave-absorbing materials (Kurt et al., 2025), polarization converters (Ozturk et al., 2023), performance-enhancing elements in antenna systems (Li et al., 2024), radar cross-section reduction structures (Alahmed Albasry et al., 2025), and sensor systems (Rashedul Islam et al., 2022).

MMA designs are generally constructed using a lossy dielectric material placed between two metallic layers. This dielectric layer plays a crucial role in the absorption of EM waves. For this purpose, dielectric materials such as FR-4 (Kurt et al., 2025), Rogers (Khalil et al., 2025), quartz (Prince & Anowar, 2025), F4-B (Kamal et al., 2023), and Arlon (Teber, 2024) are commonly used in the intermediate layer. When selecting the material to be used in this layer for MMA designs, several factors must be considered, including dielectric loss, dielectric constant, mechanical strength, cost, and ease of fabrication. FR-4 stands out due to its low cost, easy availability, and high mechanical robustness. Its compatibility with PCB (Printed Circuit Board) fabrication techniques simplifies the manufacturing process and provides a cost advantage. Additionally, its balanced structure in terms of rigidity and flexibility minimizes deformation risks and enhances structural reliability. For these reasons, FR-4 was chosen as the substrate material in this study. Rogers, on the other hand, is another dielectric material known for its low dielectric loss and stable performance at high frequencies; however, it is more expensive compared to FR-4. Quartz is preferred in precise and high-frequency applications due to its very low losses, but its brittle nature makes it difficult to process. Specialized materials such as F4-B and Arlon offer advantages in terms of low loss and stable performance, yet their high cost limits their widespread use.

While MMA's are generally realized using a metal–dielectric–metal trilayer configuration, alternative structural designs include single-layer absorbers (Zheng et al., 2024) as well as multilayer arrangements (Hasar et al., 2025). Metasurface absorber (MSA) structures can be designed with narrowband (Y. Xie et al., 2023), multiband (Luo et al., 2021), or broadband (T. Xie et al., 2022) characteristics depending on the targeted applications. To enhance broadband absorption performance, some designs integrate passive circuit elements such as resistance (R), inductance (L), and capacitance (C) into the metamaterial structure (Ardeshana et al., 2025). In other approaches, thin-film coating techniques are applied to enhance impedance matching, thereby achieving effective absorption over a wider frequency range (W. Wang et al., 2021).

In this study, a MSA operating at microwave frequencies was designed by utilizing the EM wave absorption capability of metamaterials. The developed MSA aims to absorb incident EM waves at specific resonance frequencies without transmission through the structure and with minimal reflection. Thus, by trapping the waves within the structure, a high-performance absorber suitable for various microwave applications is presented. The conductive (copper) layer placed on the backside of the metasurface (MS) is intended to completely block EM transmission and achieve zero transmission ($S_{21}$) The resonator structure on the front side and the dielectric material in the intermediate layer play a crucial role in controlling the reflection coefficient ($S_{11}$) Accordingly, the dielectric properties and resonator geometry were carefully optimized to ensure effective absorption.

The primary aim of this study is to design and evaluate an MSA operating at microwave frequencies that exhibits high absorption, features a structurally thin profile, and offers ease of fabrication.

Within this context, a comprehensive literature review was conducted, and the proposed MSA was systematically compared MSA was systematically compared against existing works based on multiple criteria, including the number of absorption bands, maximum absorption efficiency, material composition, structural thickness, and performance under varying incident angles. The comparative analysis demonstrates that the designed MSA outperforms analogous structures reported in the literature in terms of these parameters, thereby providing an enhanced absorption capability suitable for advanced microwave applications.

## 2. Material and Methods

Figure 1(a–b) shows the unit cell structure of the proposed quad-band MSA and the positions of its geometric parameters, modeled using CST Microwave Studio. The design uses copper for both the top and bottom layers, with an electrical conductivity of $5.8\times10^7$ S/m. The middle layer is made of an FR-4 dielectric substrate, which has a relative permittivity $\varepsilon_r$=4.3, relative permeability of $\mu_r$= 1, and a loss tangent of tanδ = 0.025. The copper layers are each 0.035 mm thick, and the FR-4 substrate has a thickness of 1 mm.

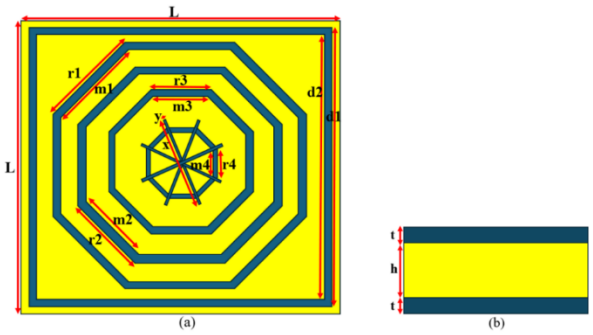



**Figure 1:** Schematic view of the MSA unit cell

The geometric parameters of the proposed MSA structure are as follows: L = 8.8 mm, d1 = 8.6 mm, d2 = 8.2 mm, r1 = 3.14 mm, m1 = 2.91 mm, r2 = 2.53 mm, m2 = 2.3 mm, r3 = 1.76 mm, m3 = 1.53 mm, r4 = 0.99 mm, m4 = 0.77 mm, t = 0.035 mm, h = 1 mm, x = 3 mm, and y = 0.1 mm.

Scattering parameters (S-parameters) are commonly used to analyze the EM responses (reflection and transmission characteristics) at microwave frequencies. Using S-parameters, the absorption function A(ω) of the MSA can be obtained as shown in Equation (1-2) (Hakim et al., 2021).

$$A(\omega) = 1 - |S_{11}(w)|^2 - |S_{21}(w)|^2 \qquad (1)$$

$$A(w) = 1 - R(\omega) - T(\omega) \qquad (2)$$

In this context, A(ω) represents the frequency-dependent absorption ratio of the MS structure; $|S_{11}(\omega)|^2$ corresponds to the reflected component, and $|S_{21}(\omega)|^2$ represents the transmitted EM wave component. Since the bottom layer of the proposed metal–dielectric–metal structure is fully coated with a conductive material (copper), the transmission of EM waves through the structure becomes effectively zero. Therefore, the $S_{21}(\omega)$ parameter can be considered negligible, and the transmission through the structure is approximately zero. Under this condition, the absorption ratio can be associated solely with the reflection component, making the expression A(ω) = 1 – R(ω) valid.

To confirm the metamaterial properties of the proposed MS unit cell, precise determination of the structure's electric permittivity and magnetic permeability parameters is essential. The Nicolson–Ross–Weir (NRW) technique was selected for extracting these EM parameters owing to its straightforward implementation and proven analytical reliability. The Nicolson–Ross–Weir (NRW) method enables precise extraction of the material's relative electric permittivity ($\varepsilon_r$), magnetic permeability ($\mu_r$), refractive index ($n_r$), and normalized impedance ($Z_r$) based on the simulated reflection ($S_{11}$) and transmission ($S_{21}$) scattering parameters of the structure. The relevant parameter retrieval calculations were performed according to the mathematical expressions detailed in Equations (3–6) (Billa et al., 2024).

$$\varepsilon_r = \frac{2}{jwd}\frac{1-(S_{21+}S_{11})}{1+(S_{21+}S_{11})} \qquad (3)$$

$$\mu_r = \frac{2}{jwd}\frac{1-(S_{21-}S_{11})}{1+(S_{21-}S_{11})} \qquad (4)$$

$$n_r = \frac{c}{j\pi fd}\sqrt{\frac{(S_{21-}1)^2-(S_{11})^2}{(S_{21}+1)^2-(S_{11})^2}} \qquad (5)$$

$$Z_r = \sqrt{\frac{\mu_r}{\varepsilon_r}} = \sqrt{\frac{(1+S_{11})^2-(S_{21})^2}{(1-S_{11})^2-(S_{21})^2}} \qquad (6)$$

## 3. Results and Discussion

This study assessed the EM behavior of the proposed MSA through simulations performed in CST Microwave Studio (CST). During the simulation process, unit cell boundary conditions were applied assuming that the structure is periodically repeated infinitely, and Floquet modes were defined to perform the analyses in the frequency domain. The MSA was illuminated by a plane EM wave, where the electric field (E) points along the y-axis, the magnetic field (H) along the x-axis, and the wave vector (k) along the z-axis, covering frequencies from 1 to 18 GHz. These settings approximate practical operating conditions (normal incidence, periodic array), improving the relevance of the simulation results. The simulation results are shown in Figure 2. According to the data, the absorber reaches absorption rates of 99.8%, 99.9%, 96.9%, and 99.02% at 3.5 GHz, 7.1

GHz, 9.4 GHz, and 13.7 GHz, respectively, corresponding to the S, C, X, and Ku frequency bands.

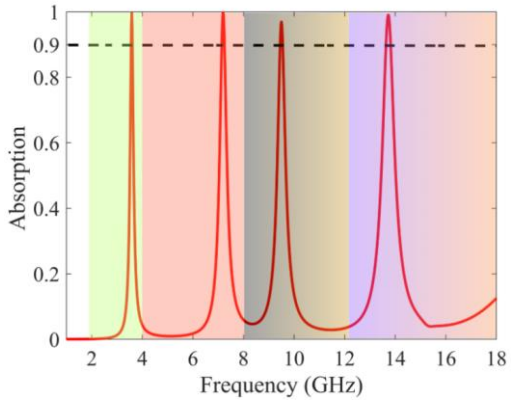



**Figure 2:** Absorption performance of the unit cell simulated by CST

In MSAs developed for microwave applications, maintaining high absorption performance despite EM waves incident from different incident angles is crucial. Figure 3(a-b) presents the absorption performance of the proposed MSA under TE and TM modes at various polarization angles (Ø= 0°, 30°, 60° and 90°). In both modes, the absorption profile does not change with respect to the polarization angle. This indicates that the structure operates independently of polarization. In addition to these results, Table 1 provides detailed resonance absorption values for the TE mode under different polarization angles, while Table 2 presents the resonance absorption values for the TM mode. These tables confirm, through numerical data, the polarization independence observed in the graphical results.

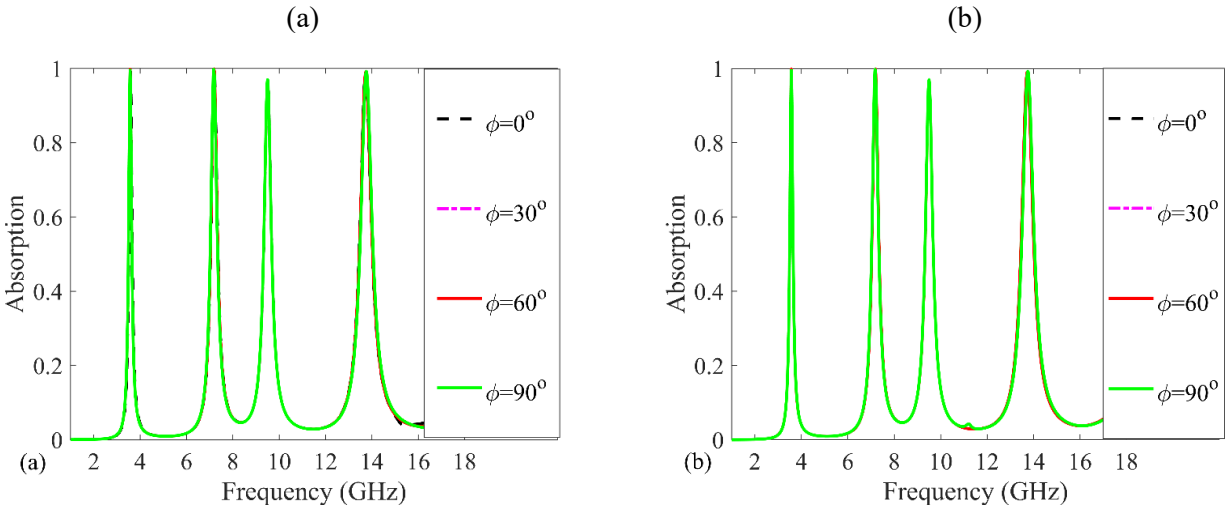



**Figure 3:** Effect of polarization angle variations on the absorption spectrum: (a) TE mode, (b) TM mode.

**Table 1:** Resonance absorption values for TE-mode under different polarization angles.

| TE Mode | Resonance Frequency (GHz) Absorption Rate | | | |
|---|---|---|---|---|
| Ø = 0° | 3,5 GHz %99,8 | 7,1 GHz %99,9 | 9,4 GHz %96,9 | 13,7 GHz %99 |
| Ø = 30° | 3,5 GHz %99,4 | 7,1 GHz %98,8 | 9,4 GHZ %95,2 | 13,7 GHz %98,5 |
| Ø = 60° | 3,5 GHz %98,8 | 7,2 GHz %98,2 | 9,5 GHZ %90,2 | 13,6 GHz %96,5 |
| Ø = 90° | 3,5 GHz %97,4 | 7,2 GHz %95,7 | 9,5 GHZ %94,8 | 13,6 GHz %96,4 |

**Table 2:** Resonance absorption values for TM-mode under different polarization angles.

| TM Mode | Resonance Frequency (GHz) Absorption Rate | | | |
|---|---|---|---|---|
| Ø = 0° | 3,5 GHz %99,8 | 7,1 GHz %99,9 | 9,4 GHz %96,9 | 13,7 GHz %99,02 |
| Ø = 30° | 3,5 GHz %99,4 | 7,1 GHz %98,8 | 9,4 GHZ %95,2 | 13,71 GHz %98 |
| Ø = 60° | 3,5GHz %98,8 | 7,2 GHz %98,2 | 9,5 GHZ %90,24 | 13,68 GHz %96,5 |
| Ø = 90° | 3,5 GHz %97,4 | 7,2 GHz %95,68 | 9,5 GHZ %94,8 | 13,6 GHz %96,4 |

Figure 4(a–b) presents the absorption performance of the proposed MSA under TE and TM modes for incident angles ranging from 0° to 75° with increments of 15°. The detailed absorption values corresponding to the oblique incidence angles in the TE mode shown in Figure 4(a) are provided in Table 3, while the detailed results for the TM mode presented in Figure 4(b) are given in Table 4. The findings indicate that the absorber maintains an absorption level above 80% up to an incident angle of 60°, demonstrating high stability against variations in the angle of incidence.

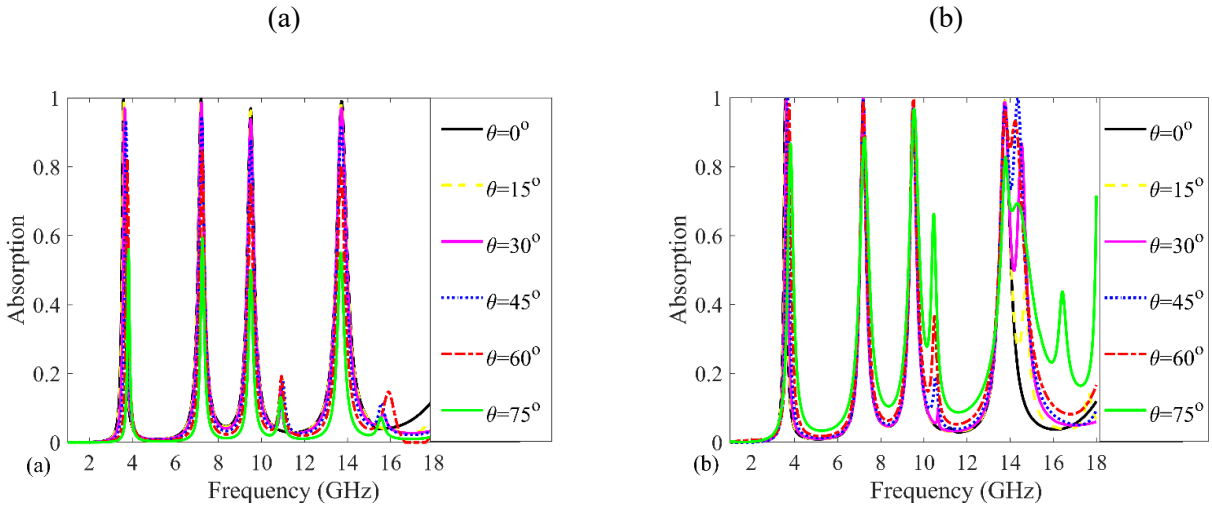



**Figure 4:** Absorption performance of the MSA under different incident angles: (a) TE mode, (b) TM mode

**Table 3:** Resonance absorption values for the TE mode under different oblique incidence angles.

| TE Mode | Resonance Frequency (GHz) Absorption Rate | | | |
|---|---|---|---|---|
| $\theta = 0^{\circ}$ | 3,5 GHz %99,8 | 7,1 GHz %99,9 | 9,4 GHz %96,9 | 13,7 GHz %99 |
| $\theta = 15^{\circ}$ | 3,5 GHz %99,4 | 7,1 GHz %99 | 9,4 GHz %95,2 | 13,7 GHz %98,5 |
| $\theta = 30^{\circ}$ | 3,6 GHz %96,8 | 7,2 GHz %98,2 | 9,5 GHz %90,2 | 13,6 GHz %96,5 |
| $\theta = 45^{\circ}$ | 3,7 GHz %93,4 | 7,2 GHz %94,7 | 9,5 GHz %87,8 | 13,6 GHz %92 |
| $\theta = 60^{\circ}$ | 3,8 GHz %82 | 7,2 GHz %86,1 | 9,5 GHz %80,2 | 13,6 GHz %80,7 |
| $\theta = 75^{\circ}$ | 3,8 GHz %56 | 7,2 GHz %59,3 | 9,5 GHz %49,4 | 13,6 GHz %54,9 |

**Table 4:** Resonance absorption values for the TM mode under different oblique incidence angles.

| TM Mode | Resonance Frequency (GHz) Absorption Rate | | | |
|---|---|---|---|---|
| $\theta = 0^{\circ}$ | 3,5 GHz %99,8 | 7,1 GHz %99,9 | 9,4 GHz %96,9 | 13,7 GHz %99 |
| $\theta = 15^{\circ}$ | 3,5 GHz %99,7 | 7,1 GHz %99,2 | 9,4 GHz %94,8 | 13,7 GHz %98,66 |
| $\theta = 30^{\circ}$ | 3,6 GHz %96,8 | 7,2 GHz %98,2 | 9,5 GHz %91,2 | 13,6 GHz %97,5 |
| $\theta = 45^{\circ}$ | 3,7 GHz %98,4 | 7,2 GHz %97,7 | 9,5 GHz %95,6 | 13,6 GHz %97,4 |
| $\theta = 60^{\circ}$ | 3,8 GHz %97,3 | 7,2 GHz %96,5 | 9,5 GHz %80,2 | 13,6 GHz %95 |
| $\theta = 75^{\circ}$ | 3,8 GHz %84,2 | 7,2 GHz %84,2 | 9,5 GHz %90 | 13,8 GHz %77,4 |

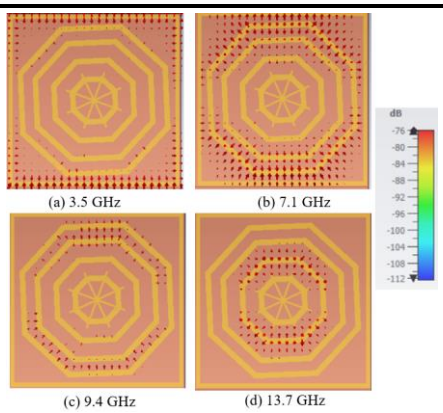



**Figure 5:** E distribution presentations for the proposed unit cell MSA.

To gain deeper insight into the working principle of the proposed MSA, the E, H, and surface current distributions were analyzed at 3.5 GHz, 7.1 GHz, 9.4 GHz, and 13.7 GHz. Figure 5 shows the E patterns at these frequencies. The red areas in the images highlight where the E is strongest, indicating resonance regions where the structure absorbs and dissipates EM energy.

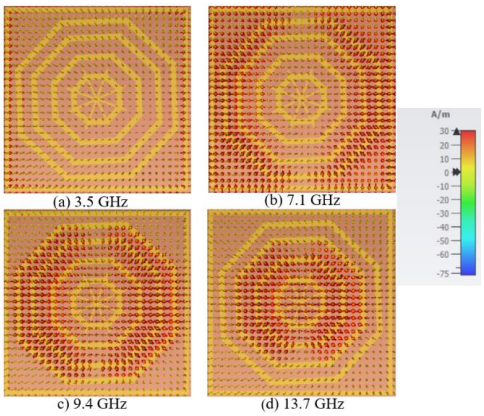



**Figure 6:** H distribution presentations for the proposed unit cell MSA.

When compared with Figure 5, it is observed that the E and H intensities are concentrated in different regions of the unit cell at the same resonance frequencies. This distribution confirms that the electric and magnetic fields exhibit sinusoidal variation and are oriented in mutually perpendicular directions, consistent with the nature of electromagnetic wave propagation. Figure 7 presents the surface current distributions of the designed MSA. When these distributions are compared with the H distributions in Figure 6, it is observed that the current densities are formed in regions where the H is strong and occur at the same frequency points. This demonstrates the relationship between surface currents and H and supports Maxwell's equations.

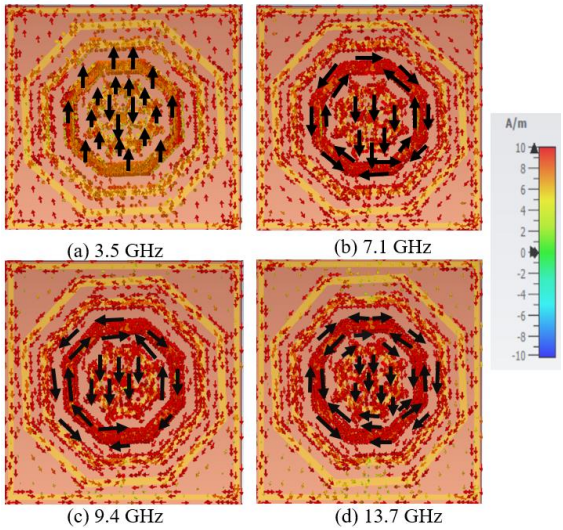



**Figure 7:** Surface current distribution presentations for the proposed unit cell MSA.

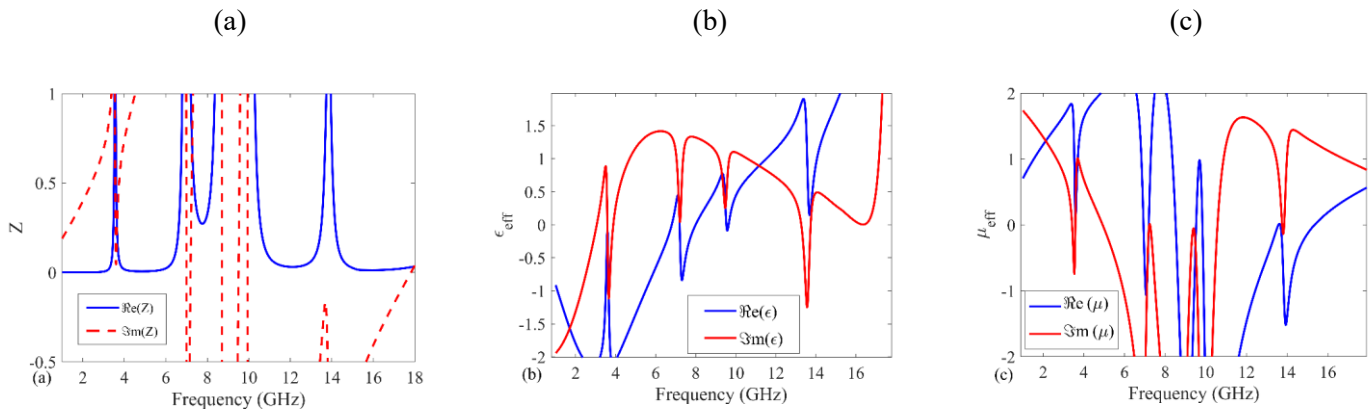



**Figure 8:** Frequency-dependent variations of the proposed MSA's (a) normalized impedance, (b) effective electric permittivity (ε), and (c) effective magnetic permeability (μ) graphs

To analyze the metamaterial behavior, the expressions given in Equations (3–6) were integrated into the MATLAB program, and graphs of the normalized impedance as well as the effective electric

and magnetic permittivity were obtained and evaluated. Figure 8(a) shows the frequency-dependent variation of the normalized input impedance of the proposed MSA. The real part of the input impedance approaching one and the imaginary part approaching zero indicates that the structure achieves impedance matching with free space, resulting in high absorption at specific frequencies. Figures 8(b–c) present the electric permittivity and magnetic permeability values, respectively. The presence of negative values in either ε or μ within certain frequency ranges indicates that the structure exhibits ENG (epsilon-negative) or MNG (mu-negative) characteristics. This confirms the metamaterial behavior that forms the foundation of the absorption mechanism.

To verify the simulation results of the proposed metasurface absorber, an equivalent circuit model (ECM) of the unit cell was implemented in ADS. The circuit parameters were optimized to match the targeted resonance frequencies. The ECM is shown in Figure 9, and the detailed component values are listed in Table 5. Figure 10 presents a comparison between the reflection coefficient ($S_{11}$) responses obtained from ADS and CST Microwave Studio. The good agreement observed at the resonance frequencies confirms the validity of the equivalent circuit model and supports the accuracy of the proposed design.

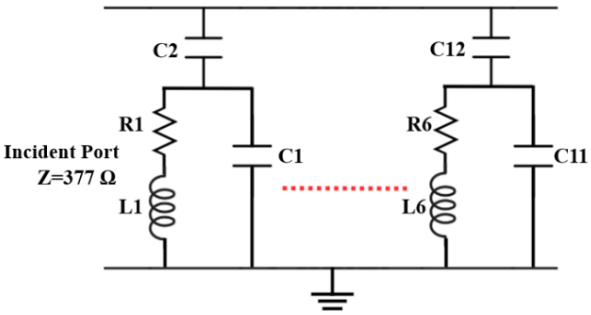



**Figure 9:** ECM of the proposed MSA

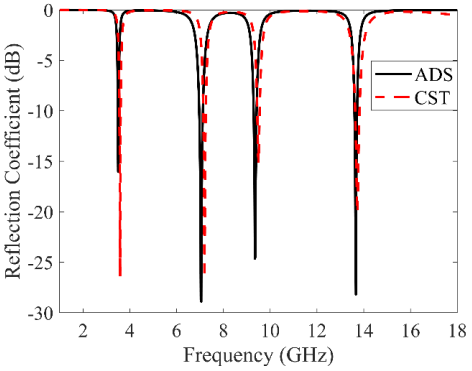



**Figure 10:** Reflection coefficient of the proposed MSA from ADS and CST results

**Table 5:** Component values used in the ECM of the proposed MSA.

| Resistance (Ω) | Inductance (nH) | Series Capacitance (fF) | Parallel Capacitance (fF) |
|---|---|---|---|
| R1=12.6641 | L1=8.82691 | C1=46.0986 | C2=13.0426 |
| R2=14.289 | L2=33.6335 | C3=50.363 | C4=11.1959 |
| R3=11.8661 | L3=9.6951 | C5=23.7446 | C6=6.54686 |
| R4=10.6982 | L4=6.28955 | C7=1120140 | C8=5.77645 |
| R5=12.6751 | L5=12.2318 | C9=8.11268 | C10=3.14665 |
| R6=9.36673 | L6=7.2046 | C11=2.2441 | C12=3.9155 |

According to the comparison presented in Table 6, the proposed MSA demonstrates superior performance compared to the other study (Errajraji et al., 2025) by achieving over 95% success in absorption rate at all resonance frequencies. It has a higher number of bands compared to the other study (Afsar et al., 2024). Its ability to operate at four different frequencies simultaneously indicates that it is more functional in terms of operating frequency than the other studies in the literature (Afsar et al., 2024; Binda et al., 2023; Ila & Yaldiz, 2024; Jahan et al., 2023). The use of FR-4 material in the proposed MSA offers a more cost-effective and production-friendly structure compared to the other study (Jahan et al., 2023). Additionally, it exhibits satisfactory oblique incidence performance up to 60°. Considering all these features, the proposed MSA stands out from similar designs in the literature with its high absorption rate, multi-band operation capability, ease of fabrication, and low-cost structure.

**Table 6:** Comparison of the proposed MSA with similar structures in the literature.

| Reference | Resonance Frequency (GHz)-Absorption Rate | Operating Frequency | Number of Bands | Material | Thickness | Incident Angle |
|---|---|---|---|---|---|---|
| (Binda et al., 2023) | 5.026 (%95.67), 8.582 (%99.16), 11.73 (%95.97)and 15.036 (%97.02) | C, X and Ku | 4 | FR-4 | 0.8 mm $\lambda$=0.0134$\lambda_0$ | TE=30 TM=60 |
| (Jahan et al., 2023) | 4.87 (%99.9), 7.49 (%99.9), 11.78 (%99.9) and 13.09 (%99.8) | C,X and Ku | 4 | Rogers RT5870 | 1,575 mm $\lambda$=0.025$\lambda_0$ | - |
| (Ila & Yaldiz, 2024) | 2.01 (%99.79), 3.51 (%98.84), 7.26 (%99.86) and 9.41 (%98.98) | S, C and X | 4 | FR-4 | 1.6 mm $\lambda$=0.0107$\lambda_0$ | 60 |
| (Afsar et al., 2024) | 3.02 (%99.86), 5.71 (%97.58) and 8.36 (%97.46) | S, C and X | 3 | FR-4 | 1.6 mm $\lambda$=0.016$\lambda_0$ | 75 |
| (Errajraji et al., 2025) | 3.84 (%98.49), 7.41 (%95.94), 10.56 (%94.00) and 15.66 (%99.88) | S,C,X and Ku | 4 | FR-4 | 0.8 mm $\lambda$=0.0102$\lambda_0$ | 60 |
| This work | 3.5 (%99.8), 7.1 (%99.9), 9.4 (%96.9) and 13.7 (%99.02) | S,C,X and Ku | 4 | FR-4 | 1 mm $\lambda$=0.011$\lambda_0$ | 60 |

## 4. Conclusion

In this study, a four-band MSA operating in the S, C, X, and Ku frequency bands was designed. The absorber showed high absorption rates of 99.8%, 99.9%, 96.9%, and 99.02% at 3.5 GHz, 7.1 GHz, 9.4 GHz, and 13.7 GHz, respectively. Similar performance was observed for both TE and TM polarizations, indicating that the design is polarization insensitive. Additionally, tests at different angles of incidence revealed that the absorption remained above 80% up to 60°. To further verify the simulation results, an ECM of the unit cell was created and simulated using ADS software. The ADS model results showed strong agreement with the CST simulations, confirming the accuracy of the study. This consistency supports the reliability of the design and its potential for practical applications.

## Article Information

**Financial Disclosure:** The author (s) has not received any financial support for the research, authorship or publication of this study.

**Authors' Contribution:** Concept: M.K.; Design: M.K; Supervision: G.Ö; Resources: M.K; Data Collection: M.K; Analysis: M.K., G.Ö.; Literature Search: M.K., G.Ö.; Writing Manuscript: M.K.; Critical Review: G.Ö

**Conflict of Interest/Common Interest:** No conflict of interest or common interest has been declared by the authors.

**Ethics Committee Approval:** This study does not require ethics committee permission or any special permission.

**Artificial Intelligence Statement:** The author(s) bear full responsibility for the content and accuracy of their work, including any use of artificial intelligence (AI) technologies, and confirm that they have read the AI Policy, which is accessible on the journal's website.

## References

Afsar, M. S. U., Faruque, M. R. I., Abdullah, S., & Hossain, M. J. (2024). Rotational symmetric solar system shaped triple band perfect metamaterial absorber for S-, C-, and X-band application. *Sensors and Actuators A: Physical*, *365*. https://doi.org/10.1016/j.sna.2023.114839

Alahmed Albasry, F., Ozturk, G., Hasar, U. C., & Corapsiz, M. F. (2025). Ultra-Thin Metasurface Polarization Converter with Linear and Circular Polarization Features for RCS Applications. *Arabian Journal for Science and Engineering*, *50*, 5463–5473. https://doi.org/10.1007/s13369-024-09358-y

Ardeshana, M. A., Thakkar, F. N., & Domadia, S. G. (2025). Composite structure design for broadband metamaterial absorption: Integrated nonlinearity and enhanced performance using lumped resistors. *Journal of Applied Physics*, *137*. https://doi.org/10.1063/5.0250746

Billa, M. B., Alam, T., Islam, M. T., Misran, N., Islam, M. R., Hakim, M. L., Alrashidi, A., & S Soliman, M. (2024). Polarization insensitive multiband metamaterial absorber for bio-plastic sensing application. *Materials Today Sustainability*, *26*. https://doi.org/10.1016/j.mtsust.2024.100738

Binda, P., Singh, R. K., & Mitharwal, R. (2023). An ultra-thin, polarization free wide-angle stable quad-band metamaterial absorber for applications in C, X, and Ku bands. *AEU - International Journal of Electronics and Communications*, *171*. https://doi.org/10.1016/j.aeue.2023.154925

Chen, J., Chen, J., Wang, H., He, L., Huang, B., Dadbakhsh, S., & Bartolo, P. (2025). Fabrication and development of mechanical metamaterials via additive manufacturing for biomedical applications: a review. In *International Journal of Extreme Manufacturing* (Vol. 7). Institute of Physics. https://doi.org/10.1088/2631-7990/ad88e3

Errajraji, K., Das, S., Jebbor, N., Ali, W., Islam, T., & El-Arrouch, T. (2025). Design of an ultra-thin quad-band metamaterial absorber for sensing and antenna performance enhancement. *Measurement: Journal of the International Measurement Confederation*, *242*. https://doi.org/10.1016/j.measurement.2024.116027

Hakim, M. L., Alam, T., Almutairi, A. F., Mansor, M. F., & Islam, M. T. (2021). Polarization insensitivity characterization of dual-band perfect metamaterial absorber for K band sensing applications. *Scientific Reports*, *11*. https://doi.org/10.1038/s41598-021-97395-0

Hasar, U. C., Kaya, Y., Korkmaz, H., & Iliev, T. (2025). Broadband Multilayer Absorber Design Using Double-Stage Cognitive Seeker Optimization Algorithm. *IEEE Access*, *13*, 27178–27190. https://doi.org/10.1109/ACCESS.2025.3537661

Ila, B., & Yaldiz, E. (2024). Quad-Band Incident Angle Insensitive Metamaterial Absorber for S, C and X-Band Applications. *2024 18th International Congress on Artificial Materials for Novel Wave Phenomena, Metamaterials 2024*. https://doi.org/10.1109/Metamaterials62190.2024.10703235

Jahan, M. I., Faruque, M. R. I., Hossain, M. B., Khandaker, M. U., Elsayed, F., Salman, M., & Osman, H. (2023). Quad-Band Metamaterial Perfect Absorber with High Shielding Effectiveness Using Double X-Shaped Ring Resonator. *Materials*, *16*. https://doi.org/10.3390/ma16124405

Kamal, B., Khan, B., Chen, J., Yin, Y., Ren, J., & Ullah, S. (2023). Ultra-Thin Wideband Polarization Converting Metasurface for Complete KU and K Bands Microwave Applications. *Proceedings of 2023 IEEE International Conference on Signal Processing, Communications and Computing, ICSPCC 2023*. https://doi.org/10.1109/ICSPCC59353.2023.10400313

Khalil, M. A., Islam, M. T., Yong, W. H., Islam, M. S., Goh, H. H., Kurniawan, T. A., Rehman Junejo, N. U., Soliman, M. S., & Khawaja, A. W. (2025). Design and validation of a multi-band metamaterial absorber for microwave applications. *AEU - International Journal of Electronics and Communications*, *193*. https://doi.org/10.1016/j.aeue.2025.155718

Kurt, M., Ozturk, G., & Ertugrul, M. (2025). Hepta-Band Ultra-Thin Metasurface Absorber for S-, C-, X-, Ku-, and K-Band Applications. *Arabian Journal for Science and Engineering*. https://doi.org/10.1007/s13369-025-10140-x

Landy, N. I., Sajuyigbe, S., Mock, J. J., Smith, D. R., & Padilla, W. J. (2008). Perfect metamaterial absorber. *Physical Review Letters*, *100*. https://doi.org/10.1103/PhysRevLett.100.207402

Li, W., Zhang, kun, Pei, R., & Xu, F. (2024). Composite metamaterial antenna with super mechanical and electromagnetic performances integrated by three-dimensional weaving technique. *Composites Part B: Engineering*, *273*.

https://doi.org/10.1016/j.compositesb.2024.111265

Luo, Z., Ji, S., Zhao, J., Wu, H., & Dai, H. (2021). A multiband metamaterial absorber for GHz and THz simultaneously. *Results in Physics*, *30*. https://doi.org/10.1016/j.rinp.2021.104893

Meenakshi, Saurav, P., & Kishor, K. (2022). Design and simulation of metamaterial under the THz frequency for short-range wireless communication and military purposes. *Materials Today: Proceedings*, *62*, 3729–3733. https://doi.org/10.1016/j.matpr.2022.04.437

Ozturk, G., Hasar, U. C., Ertugrul, M., Tutar, F., Corapsiz, M. F., Kurt, M., Donmez, K., Ismail, I., & Alfaqawi, M. S. S. (2023). An efficient cost effective wide-angle metasurface-based linear and circular polarization converter for X-, Ku- and K-band applications. *Optics and Laser Technology*, *163*. https://doi.org/10.1016/j.optlastec.2023.109404

Padilla, W. J., & Averitt, R. D. (2022). Imaging with metamaterials. In *Nature Reviews Physics* (Vol. 4, pp. 85–100). Springer Nature. https://doi.org/10.1038/s42254-021-00394-3

Pendry, J. B., Holden, A. J., Robbins, D. J., & Stewart, W. J. (1998). Low frequency plasmons in thin-wire structures. *Journal of Physics Condensed Matter*, *10*, 4785–4809. https://doi.org/10.1088/0953-8984/10/22/007

Pendry, J. B., Holden, A. J., Robbins, D. J., & Stewart, W. J. (1999). Magnetism from conductors and enhanced nonlinear phenomena. *IEEE Transactions on Microwave Theory and Techniques*, *47*, 2075–2084. https://doi.org/10.1109/22.798002

Prince, M. R. I., & Anowar, F. (2025). Design and Characterization of a Graphene Based Multi-Narrowband Metamaterial Absorber for Terahertz Application. *2025 International Conference on Electrical, Computer and Communication Engineering, ECCE 2025*. https://doi.org/10.1109/ECCE64574.2025.11013796

Rashedul Islam, M., Tariqul Islam, M., Soliman, M. S., Bais, B., Jit Singh, M., Alsaif, H., & Shabiul Islam, M. (2022). Metamaterial sensor based on reflected mirror rectangular split ring resonator for the application of microwave sensing. *Measurement: Journal of the International Measurement Confederation*, *198*. https://doi.org/10.1016/j.measurement.2022.111416

Singh, R. K., & Gupta, A. (2022). Theoretical and experimental study of angle independent conformal tri-band metamaterial absorber design for industrial and defense applications. *International Journal of RF and Microwave Computer-Aided Engineering*, *32*. https://doi.org/10.1002/mmce.23402

Teber, A. (2024). Dual-Band Terahertz Metamaterial Absorber Based on LC Resonance and Dipolar Response and Its Applications. *Advanced Theory and Simulations*, *7*. https://doi.org/10.1002/adts.202300918

Wang, W., Wang, H., Yu, P., Sun, K., Tong, X., Lin, F., Wu, C., You, Y., Xie, W., Li, Y., Yuan, C., Govorov, A. O., Muskens, O. L., Xu, H., Sun, S., & Wang, Z. (2021). Broadband thin-film and metamaterial absorbers using refractory vanadium nitride and their thermal stability. *Optics Express*, *29*, 33456. https://doi.org/10.1364/oe.439546

Wang, Y., Cui, Z., Zhu, D., & Yue, L. (2019). Composite Metamaterials for THz Perfect Absorption. *Physica Status Solidi (A) Applications and Materials Science*, *216*. https://doi.org/10.1002/pssa.201800940

Xie, T., Chen, D., Xu, Y., Wang, Y., Li, M., Zhang, Z., & Yang, J. (2022). High absorption and a tunable broadband absorption based on the fractal Technology of Infrared Metamaterial Broadband Absorber. *Diamond and Related Materials*, *123*. https://doi.org/10.1016/j.diamond.2022.108872

Xie, Y., Liu, Z., Zhou, F., Luo, X., Cheng, Z., Yang, R., Cheng, J., & Yang, G. (2023). A multifrequency narrow-band perfect absorber based on graphene metamaterial. *Diamond and Related Materials*, *137*. https://doi.org/10.1016/j.diamond.2023.110100

Zheng, R., Liu, Y., Ling, L., Sheng, Z., Yi, Z., Song, Q., Tang, B., Zeng, Q., Chen, J., & Sun, T. (2024). Ultra wideband tunable terahertz metamaterial absorber based on single-layer graphene strip. *Diamond and Related Materials*, *141*. https://doi.org/10.1016/j.diamond.2023.110713